



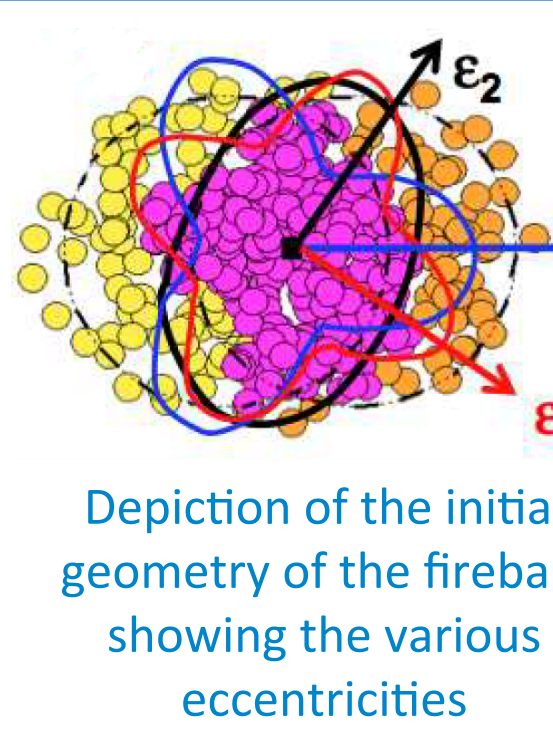
Measurement of flow harmonics in $\sqrt{s_{NN}} = 2.76 \text{ TeV}$

Pb+Pb Collisions with the ATLAS detector

Soumya Mohapatra (SUNY Stony Brook) for the ATLAS Collaboration



Motivation



In heavy ion collisions, a fireball is formed that expands collectively due to large pressure gradient and low viscosity. The azimuthal distribution of emitted particles reflects the shape initial geometry which fluctuate event by event

$$\frac{dN}{d\phi} \propto (1 + 2 \sum_{n=1}^{\infty} v_n \cos(n\phi - n\Psi_{RP,n})) \quad (\Psi_{RP,n} \equiv \text{direction of } n^{\text{th}} \text{ flow})$$

The correlation with geometry is global correlation, they also contribute to two-particle correlation in the following way

$$\frac{dN_{\text{pairs}}}{d\Delta\phi} \propto 1 + 2 \sum_{n=1}^{\infty} v_{n,n}^{a,b} \cos(n\Delta\phi), \text{ where } v_{n,n}^{a,b} = v_n^{a} v_n^{b}$$

We can measure v_n from single particle distribution relative to $\Psi_{RP,n}$ → Event-Plane (EP) method,

We can also measure v_n from pair correlations → Two Particle Correlation (2PC) method

Beside v_2 , higher order v_n ($n > 2$) carry important information about the medium such as the initial geometry and the viscosity and hence are important observables. e.g. Higher order flow are more sensitive to geometrical fluctuations and viscosity.

We present measurements of v_2-v_6 using the EP and 2PC methods with the ATLAS detector. We use Forward Calorimeter (FCal, $3.2 < |\eta| < 4.9$) for centrality and EP measurement, and we use the Inner Detector (ID, full ϕ coverage and $|\eta| < 2.5$, corresponding to $|\Delta\eta| < 5.0$ for pairs) for charged particles measurements

Event Plane (EP) Analysis

Reaction plane resolution

The reaction plane is obtained using the Q-vector method:

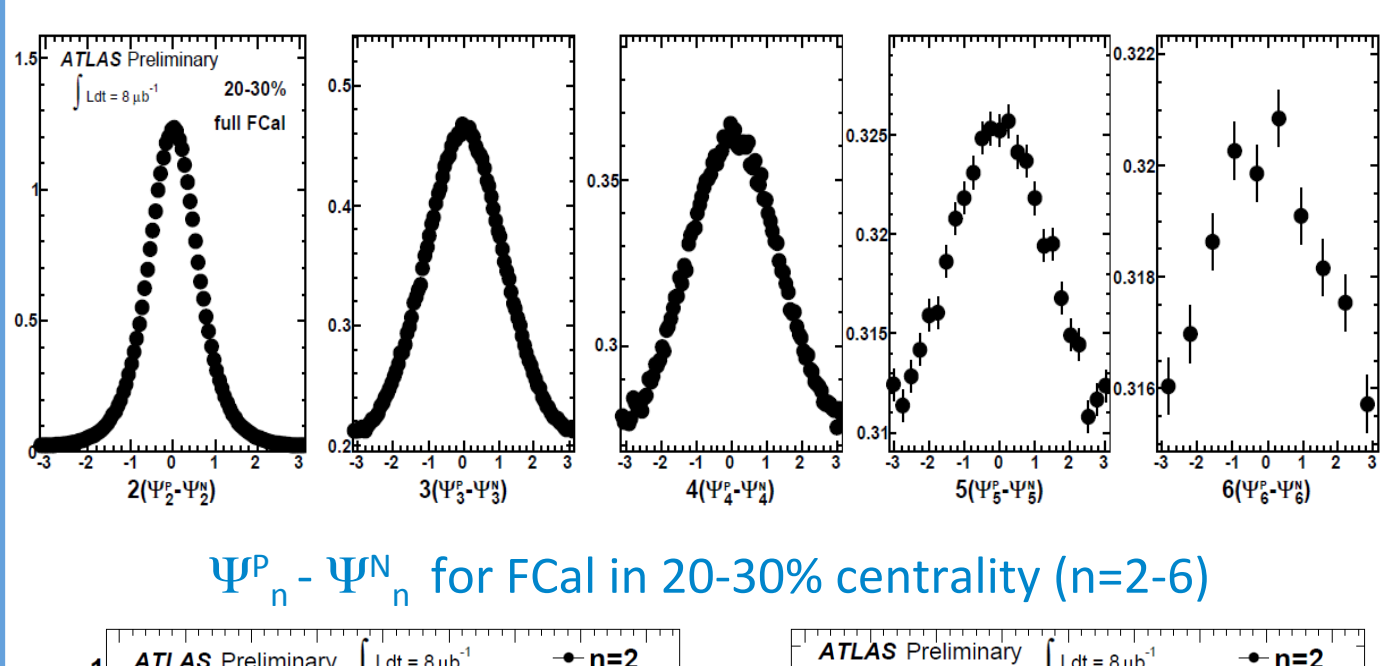
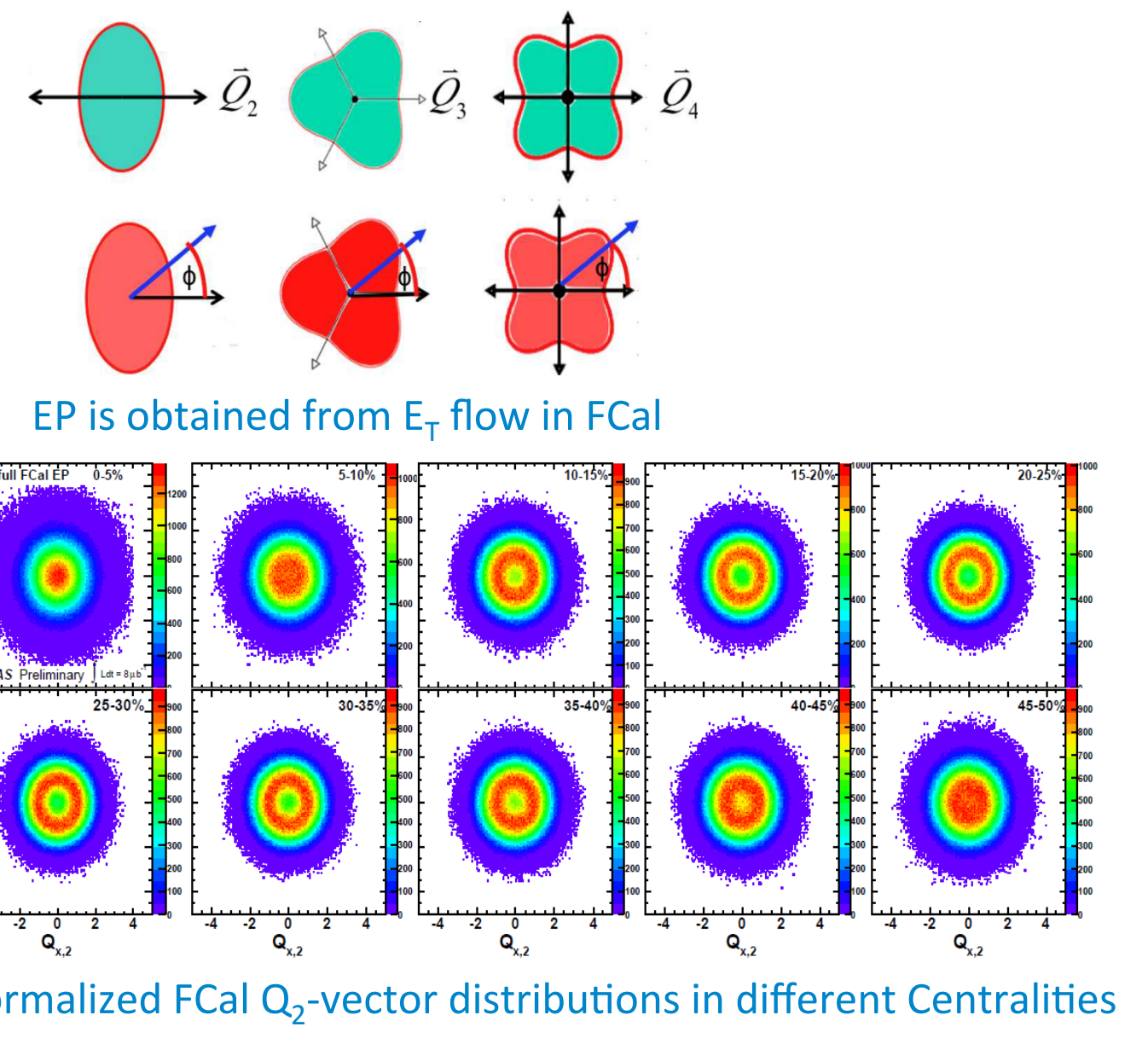
$$Q_{x,n} = \sum_i E_i \cos(n\phi_i); Q_{y,n} = \sum_i E_i \sin(n\phi_i); \Psi_n = \frac{1}{n} \tan^{-1}\left(\frac{Q_{y,n}}{Q_{x,n}}\right)$$

E_i is the energy deposited in the i^{th} FCal tower having azimuth ϕ_i .

In mid-central collisions, the Q_2 -vector is distributed in a ring-like structure indicating the excellent reaction plane resolution of the FCal.

In central and peripheral collisions and for higher orders, the ring blurs out as the resolution decreases.

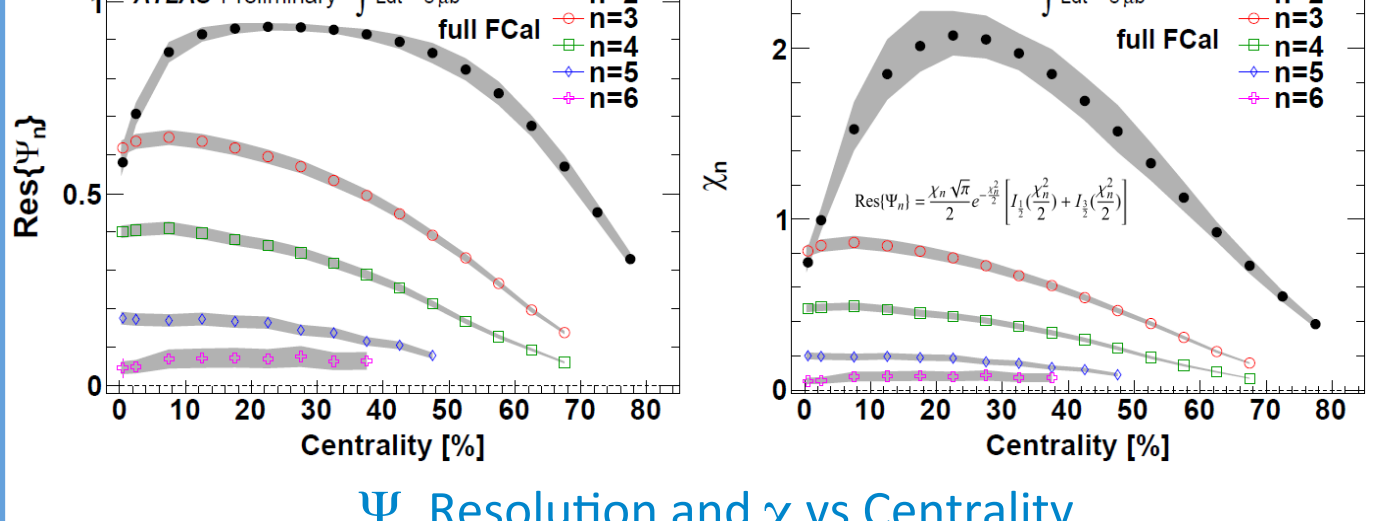
Raw v_n values are obtained by correlating tracks in Inner Detector with EP



The raw v_n are corrected to account for the FCal reaction-plane resolution:

$$v_n = \text{Res}[\Psi_n] = \frac{\langle \cos n(\phi - \Psi_n) \rangle}{\langle \cos n(\Psi_n - \Psi_{RP,n}) \rangle}$$

The resolution is obtained from the two-sub-event method using the distribution of $\Psi_p - \Psi_N$ (see figure to the left), where Ψ_p (Ψ_N) are the n^{th} order reaction planes obtained by the Positive (Negative) side of the FCal

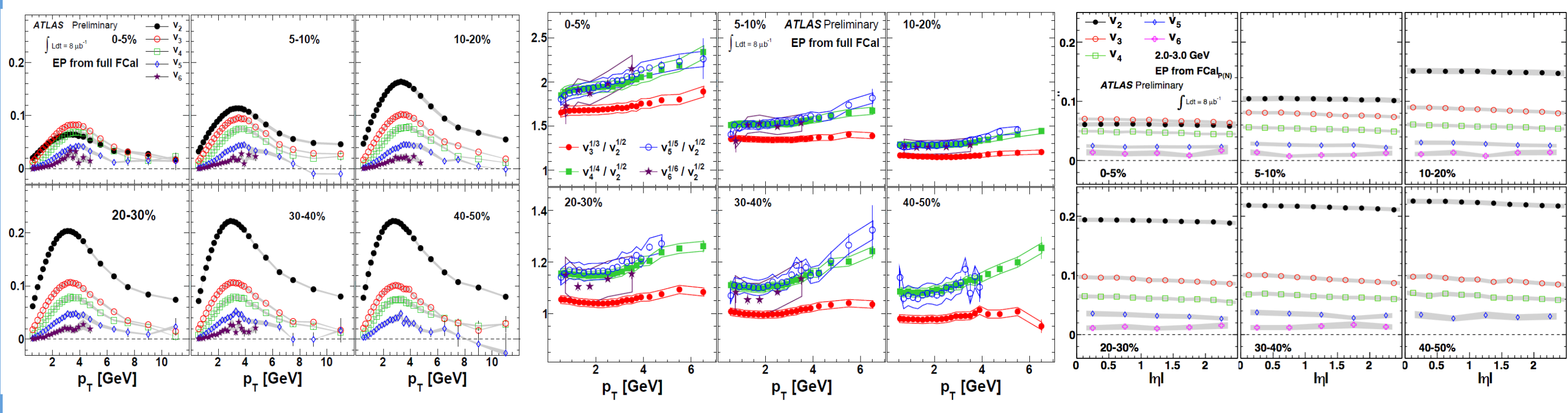


Systematic errors on the resolution are obtained by several cross-checks using the three sub-event method, where we correlate the FCal with several other detectors such as the Electromagnetic End-Cap ($1.5 < |\eta| < 3.2$), Electromagnetic Barrel ($|\eta| < 1.5$), and the Tracking detectors ($|\eta| < 2.5$)

In general the resolution for a higher order reaction plane is smaller than that of a lower order plane except in the top 1% most central events where the Ψ_3 resolution is higher than the Ψ_2 resolution.

v_n is measured for centrality selections which have good resolution (0-80% for v_2 , 0-70% for v_3 and v_4 , 0-50% for v_5 and 0-40% for v_6)

p_T and η Dependence of v_n



p_T Dependence: we see a very similar trend between all harmonics. They first increase till 3-4 GeV and then decrease.

In general the higher order harmonic is smaller than a lower order harmonic, except in the most central collisions, where v_3 and v_4 can be larger than v_2 depending on the p_T .

We also observe an interesting (approximate) scaling relation in the p_T dependence between the harmonics. We see that $v_n^{1/n} = k v_2^{1/2}$, where "k" is only weakly dependent on p_T .

η -Dependence: for all harmonics, we see only a weak dependence on η (~5% drop). This is important as it is one of the assumptions made when we try to obtain the v_n values from the two-particle correlations.

Two Particle Correlation (2PC) Analysis

2PC Method

The correlations are constructed by dividing foreground pairs by mixed background pairs.

$$C(\Delta\phi) = \frac{\text{Foreground Pairs}(\Delta\phi)}{\text{Mixed Pairs}(\Delta\phi)}$$

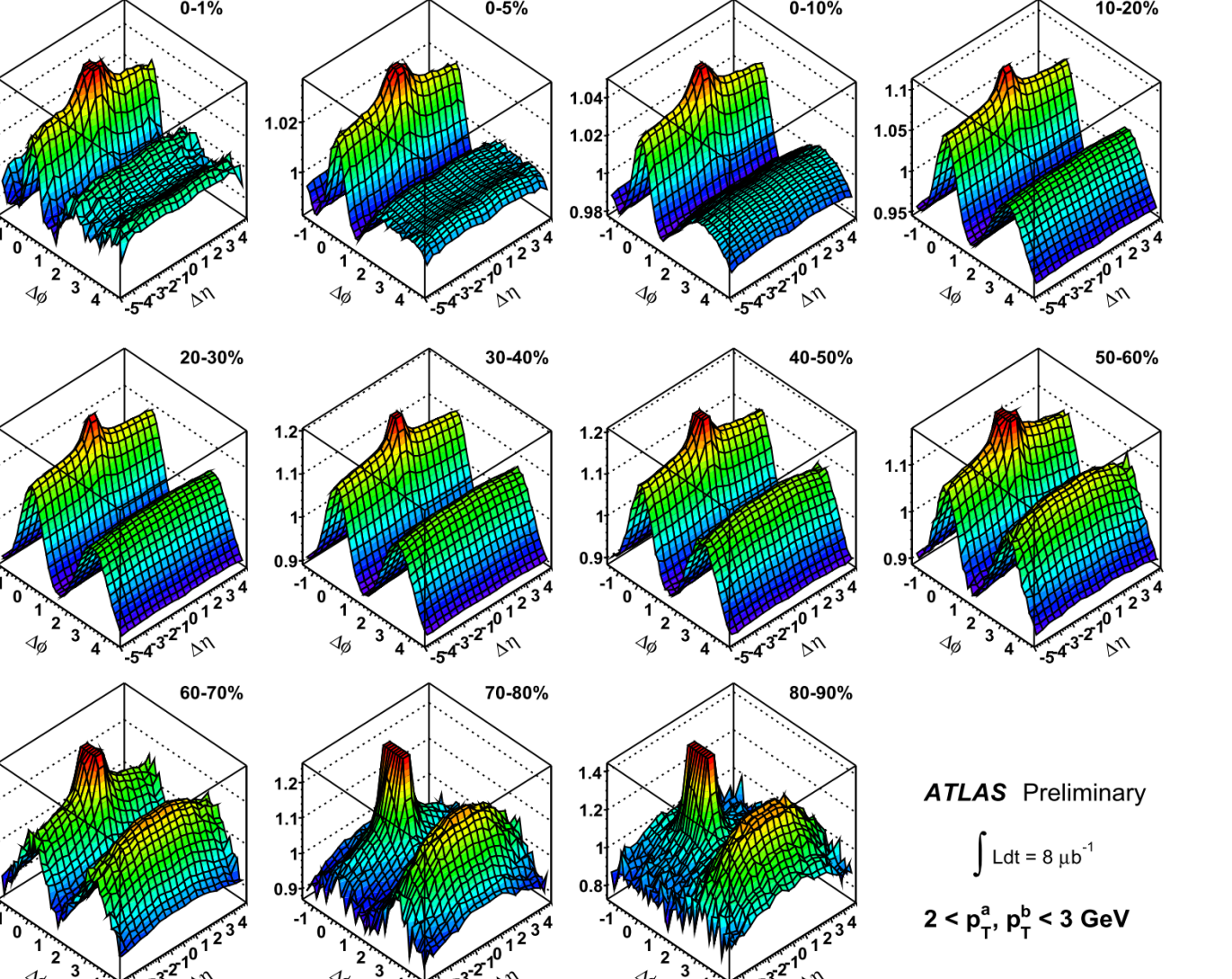
The mixed background pairs account for detector acceptance and the final correlation contains only physical effects. The figures on the right illustrate this.

The detector acceptance causes fluctuations ~ 0.001 in the foreground pairs, which mostly cancels out in the ratio.

This pair acceptance can be calculated analytically by convoluting the two single-particle acceptance functions.

They are transformed into Fourier space to quantify the influence on the $v_{n,n}$ and v_n .

Such a reconstruction is shown in the figure on the right, both in $\Delta\phi$ and in Fourier space.



Centrality and $\Delta\eta$ dependence of the correlations

Flow Harmonics From Correlations

The figures on the right show the steps in obtaining v_n

a) The 2D correlation function in $\Delta\eta, \Delta\phi$.

b) The corresponding 1D correlation function in $\Delta\phi$ for $2 < |\Delta\eta| < 5$

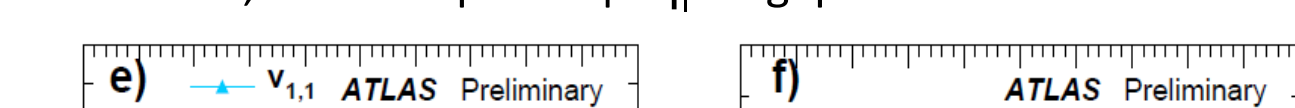
c) The $v_{n,n}$ obtained using a Discrete Fourier Transformation (DFT)

$$v_{n,n} = \langle \cos(n\Delta\phi) \rangle = \sum_{\Delta\phi} \cos(n\Delta\phi) C(\Delta\phi) / \sum_{\Delta\phi} C(\Delta\phi) \quad n=1-15$$

$$d) \text{ Corresponding } v_n \text{ values } v_n(p_T) = \sqrt{v_{n,n}(p_T, p_T)}$$

Repeat this procedure in narrow $\Delta\eta$ slices to obtain v_n vs $\Delta\eta$.

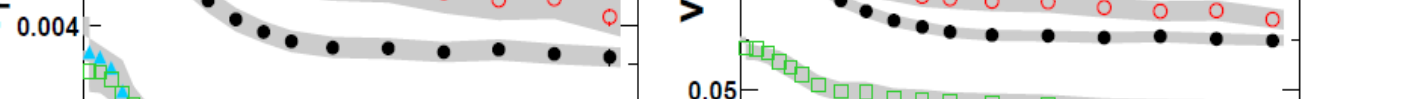
The v_n values peak at low $\Delta\eta$, due to jet bias, but are relatively flat afterwards, so we require a $|\Delta\eta| > 2$ gap.



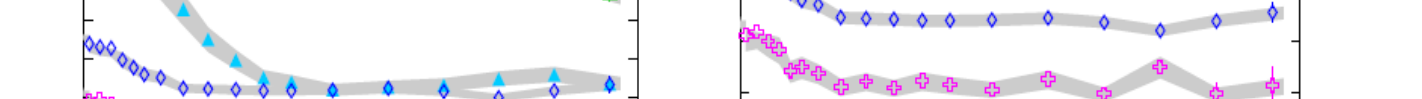
e) The $v_{n,n}$ values for $2 < p_T, p_T' < 3 \text{ GeV}$ and $0-5\%$ centrality.



f) The v_n values for $2 < p_T, p_T' < 3 \text{ GeV}$ and $0-5\%$ centrality.



g) The v_n values for $2 < p_T, p_T' < 3 \text{ GeV}$ and $2 < |\Delta\eta| < 5$.



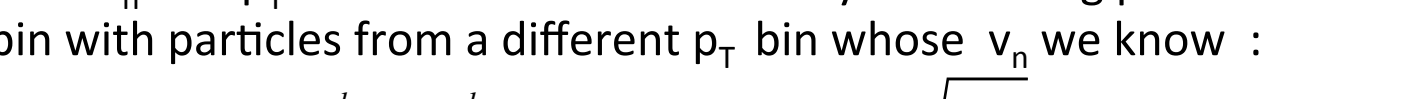
h) The v_n values for $2 < p_T, p_T' < 3 \text{ GeV}$ and $2 < |\Delta\eta| < 5$.



i) The v_n values for $2 < p_T, p_T' < 3 \text{ GeV}$ and $2 < |\Delta\eta| < 5$.



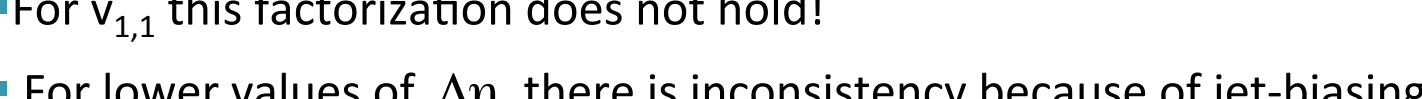
j) The v_n values for $2 < p_T, p_T' < 3 \text{ GeV}$ and $2 < |\Delta\eta| < 5$.



k) The v_n values for $2 < p_T, p_T' < 3 \text{ GeV}$ and $2 < |\Delta\eta| < 5$.



l) The v_n values for $2 < p_T, p_T' < 3 \text{ GeV}$ and $2 < |\Delta\eta| < 5$.



m) The v_n values for $2 < p_T, p_T' < 3 \text{ GeV}$ and $2 < |\Delta\eta| < 5$.



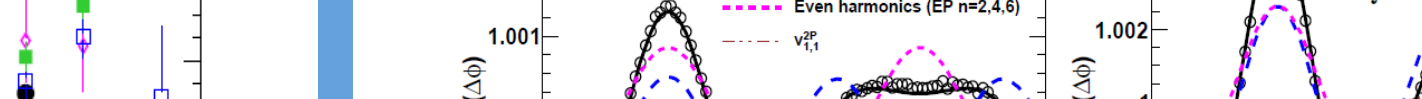
n) The v_n values for $2 < p_T, p_T' < 3 \text{ GeV}$ and $2 < |\Delta\eta| < 5$.



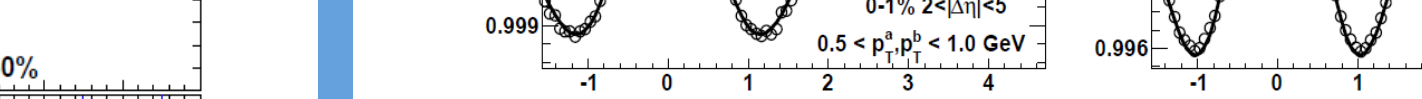
o) The v_n values for $2 < p_T, p_T' < 3 \text{ GeV}$ and $2 < |\Delta\eta| < 5$.



p) The v_n values for $2 < p_T, p_T' < 3 \text{ GeV}$ and $2 < |\Delta\eta| < 5$.



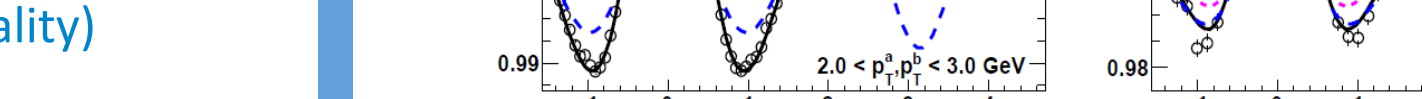
q) The v_n values for $2 < p_T, p_T' < 3 \text{ GeV}$ and $2 < |\Delta\eta| < 5$.



r) The v_n values for $2 < p_T, p_T' < 3 \text{ GeV}$ and $2 < |\Delta\eta| < 5$.



s) The v_n values for $2 < p_T, p_T' < 3 \text{ GeV}$ and $2 < |\Delta\eta| < 5$.



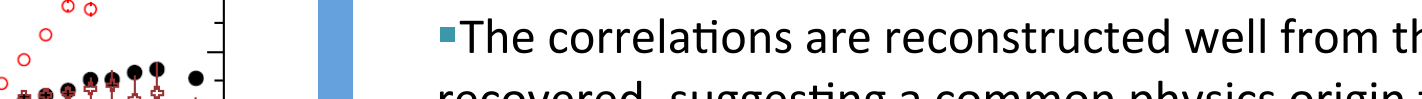
t) The v_n values for $2 < p_T, p_T' < 3 \text{ GeV}$ and $2 < |\Delta\eta| < 5$.



u) The v_n values for $2 < p_T, p_T' < 3 \text{ GeV}$ and $2 < |\Delta\eta| < 5$.



v) The v_n values for $2 < p_T, p_T' < 3 \text{ GeV}$ and $2 < |\Delta\eta| < 5$.



w) The v_n values for $2 < p_T, p_T' < 3 \text{ GeV}$ and $2 < |\Delta\eta| < 5$.



x) The v_n values for $2 < p_T, p_T' < 3 \text{ GeV}$ and $2 < |\Delta\eta| < 5$.

